Fuel 182 (2016) 304–313

Contents lists available at ScienceDirect

Fuel

journal homepage: www.elsevier.com/locate/fuel

Full Length Article

Density measurements of gasified coal and synthesized slag melts for next-generation IGCC

Arman [a,b], Akiko Okada [a], Hiromichi Takebe [a,*]

[a] Department of Materials Science and Biotechnology, Graduate School of Science and Engineering, Ehime University, 3 Bunkyo-cho, Matsuyama, Ehime 790-8577, Japan
[b] Department of Mechanical Engineering, State Polytechnic of Ujung Pandang, Jl. Perintis Kemerdekaan km. 10, Tamalanrea, 90245 Makassar, Indonesia

ARTICLE INFO

Article history:
Received 12 February 2016
Received in revised form 23 May 2016
Accepted 24 May 2016

Keywords:
IGCC
Density
Coal slag
Melt
Composition

ABSTRACT

The densities of re-melted coal slag melts were measured in air using Archimedean double-bob method in the temperature range from 1350 to 1600 °C. The main components of gasified coal slags are SiO_2, Al_2O_3, CaO, MgO, FeO and Fe_2O_3. Slags consisting of the main components with systematic composition variations were synthesized and evaluated for comparison. The experimental results of chelate titration analysis revealed that the percentages of Fe^{3+} in coal and synthesized slag samples were 47–56% and 68–80% of total Fe, respectively. The density decreased linearly with increasing temperature for all melt samples. The density of gasified and synthesized coal slag melts was found to decrease with increasing Al_2O_3 and SiO_2 contents and to increase with increasing Fe_2O_3 and FeO contents. The molar volume and the coefficient of volume expansion, which were calculated from measured density values, increased monotonically with increasing Al_2O_3 content for CaO—Al_2O_3—SiO_2 (CAS) synthesized samples with 40 mol% SiO_2. The molar volume for CaO—FeO—Fe_2O_3—SiO_2 (CFS) synthesized samples with 60 mol% SiO_2 increased with Fe_2O_3 addition and exhibited discontinuous change at ~7.5 mol% Fe_2O_3. The coefficient of volume expansion in the same CFS series decreased with increasing Fe_2O_3 content showing a minimum value at ~7 mol% Fe_2O_3 and increased in higher Fe_2O_3 content. A composition parameter calculated from chemical composition was proposed to predict the density of coal slag melts. The relationship between measured density and the composition parameter was analyzed.

1. Introduction

In view of high efficiency and environmental compliance, integrated gasification combined cycle (IGCC) as coal-based power plant technology is expected to grow by over 40% in the next 20 years in operation worldwide [1–3]. In a NEDO project, CRIEPI (Central Research Institute of Electric Power Industry) has been designing to produce electricity by IGCC with CO_2 capture [4]. The CRIEPI has used various coals with different compositions that depends on geographic origin and has set a goal to be applied a variety of coal grades in a next-generation IGCC project [5].

In the IGCC, the gasification temperature range for fluid-bed gasifiers is from 900 to 1050 °C and that for entrained-flow gasifiers is from 1200 to 1600 °C [6]. The coal is heated in the gasifier to convert the solid combustible mixture into the cleaned gases composed of CO, H_2 and CO_2 as a fuel for the IGCC gas-turbine [2,4]. The slag melts are then discharged through a hole under the gasifier and rapidly cooled by quenching in water as a gasified coal slag [7,8]. The gasification process applied to a variety of coal grades is expected to flow down the coal slag melts stably and continuously into the slag bath. Therefore, it is essential to understand the composition and temperature dependences of physical properties of coal slag melts, e.g., density, viscosity, surface tension [9–13].

Large numbers of studies concerning composition and temperature dependences of viscosity were reported for synthesized and gasified coal slag melts. Various experimental results [5,7,8,12–16] and models [17–19] have been proposed to estimate viscosity of slag melts according to coal slag composition. Limited studies on reliable data of density and surface tension have been reported for coal slag melts.

The density data is used to calculate molar volume and coefficient of volume expansion in order to discuss the molecular structure of slag melts [20–22]. The coefficient of volume expansion is one of important physical properties to control the melting process of slag melts [23,24]. Density measurements at high temperatures have been mainly carried out using maximum bubble pressure, pycnometer and Archimedean single- or double-bob methods [25–29]. The Archimedean methods give reproducible data sets

* Corresponding author.
E-mail address: takebe.hiromichi.mk@ehime-u.ac.jp (H. Takebe).

http://dx.doi.org/10.1016/j.fuel.2016.05.117
0016-2361/

with better precision [30]. Therefore, the Archimedean double-bob method is selected in this work.

Silicate slags consist of three-dimensional interconnected network of SiO_4 tetrahedra for SiO_2 as a network former (NWF) [20]. The basic oxides such as CaO, MgO break the silicate network to form non-bridging oxygen as network modifiers (NWM) [31]. The typical amphoteric oxides such as Al_2O_3 and Fe_2O_3 play dual roles as NWF and NWM depending on slag composition [5]. The slags formed during the coal gasification process mainly contain SiO_2, Al_2O_3, CaO, MgO, FeO and Fe_2O_3 with small amounts of Na_2O, K_2O, TiO_2, P_2O_5, SrO, MnO, and other compounds [21]. Synthesized coal slags with simplified silicate systems have been prepared to understand the role of components on melt properties [5,17,32]. The synthesized coal slags were used to discuss degree of polymerization and crystallization behavior of the melts [20].

The effects of Al_2O_3 and Fe_2O_3 on the density of CaO—Al_2O_3—SiO_2 (CAS) and CaO—Fe_2O_3—SiO_2 (CFS) slags are evaluated here as a start to study the structures of gasified coal slag melts. The behavior of Al_2O_3 and Fe_2O_3 in silicate glasses, crystals and slag melts has been widely studied by various techniques such as Raman and Mössbaeur spectroscopies and several melt properties such as viscosity, surface tension and density at high temperatures [33–40].

The previous studies have reported that Al^{3+} generally was NWF in silicate glasses, whereas compositional dependences of properties were qualitatively related to the glass structure examined by IR spectroscopy [40]. The proportions of AlO_x (x = 4, 5, 6) species were evaluated by using ^{27}Al MQ NMR spectroscopy [38]. In the CAS slag melts, behavior of adding Al_2O_3 shows the monotonic increase of molar volume as NWF in the composition region of $[Al_2O_3]/[CaO] < 1.00$ [34].

In silicate glasses and slag melts containing iron oxide, the structural role of iron oxide is still not well understood [39,41]. A previous study reported that the behavior of iron oxide species in CFS melts differs significantly from that in Na_2O—FeO—Fe_2O_3—SiO_2 (NFS) melts due to the behavior of Fe^{3+} ions [26,36]. Fe_2O_3 in NFS melts has the tetrahedral site, on the contrary, in CFS melts, it has octahedral one from the result of ^{57}Fe Mössbauer spectra [36]. Another study reported that the roles of Fe^{3+} varied with tetrahedral and octahedral sites in the CFS slag melts [34]. The Mössbauer spectra of quenched samples indicated that the site of Fe^{3+} ions varied from tetrahedral to octahedral coordination with increasing Fe_2O_3 content [35].

According to these scientific and engineering backgrounds, the objectives of this research are (i) to establish an Archimedean double-bob method to measure density of gasified coal and synthesized slag melts in silicate systems containing CaO or MgO and Al_2O_3 and/or FeO/Fe_2O_3, (ii) to study the composition and temperature dependences of density, molar volume, and the coefficient of volume expansion, (iii) to discuss the effect of Al_2O_3 and Fe_2O_3 on these properties, and (iv) to propose a composition parameter to predict the density of coal slag melts based on chemical composition.

2. Materials and methods

2.1. Sample preparation

2.1.1. Gasified coal slags

The samples provided by the CRIEPI, Japan are coal slags collected after rapid quenching with water of molten slag flowing from the gasifier. The samples are denoted as CV (Coal Valley), TH (Tanito Harum) and MA (Malinau). The samples were melted in a Pt crucible at 1600 °C for about 2 h. The density measurements were conducted in the range 1500–1600 °C to homogenous melt. Then the samples were rapidly cooled at room temperature to evaluate their chemical compositions. Table 1 shows the chemical compositions of the coal slag samples determined by X-ray fluorescence (XRF) analysis. The valence state of iron oxide was evaluated using chelate titration method in the quenched samples [42]. The major components in the coal slags are confirmed as SiO_2, Al_2O_3, CaO, MgO, FeO, and Fe_2O_3.

2.1.2. Synthesized slag samples

Table 2 shows that the batches of synthesized slag samples were divided into three series of $(60 - x)RO—xA_2O_3—40SiO_2$, $(50 - x)RO—xA_2O_3—50SiO_2$, and $(40 - x)RO—xA_2O_3—60SiO_2$ in molar ratio, where R is the alkaline earth metal: Ca and Mg; A is Al and Fe without considering the valence state of iron oxide. There are compositions containing 40, 50 and 60% SiO_2 (nominal concentration) with various contents of CaO, MgO, Al_2O_3 and Fe_2O_3. The composition series of synthesized slags were systematically varied by considering those of gasified coal slags (Table 1).

The samples were prepared from a mixture of SiO_2, Al_2O_3, $CaCO_3$, MgO, and Fe_2O_3 powders with 99.99% purity as raw materials. Mixed powders were melted in a Pt crucible between 1350 and 1600 °C for about 2 h depending on their homogenous melting temperatures. The synthesized slag melt was poured onto iron mold for cooling.

The cooled sample was crushed, then re-melted at the highest measuring temperature and was kept for 2 h before density measurements. The nominal contents used in this study are also shown in Table 2. The sample compositions are labeled by the type and molar fraction of components except for SiO_2, where C, A, and F mean respective oxides: CaO, Al_2O_3, and Fe_2O_3 and x and y are their molar fractions, as shown in Table 2. The valence state of iron was also determined experimentally in quenched samples after density measurements using chelate titration method. The experimental results of Fe^{3+}/Fe_{tot} are presented in Table 3. The FeO and Fe_2O_3 mol% are calculated from Fe^{3+}/Fe_{tot} for determining sample composition. The FeO and Fe_2O_3 contents (mol%) in quenched samples are

Table 1
Chemical composition of gasified coal slags.

Element	mol% (mass %)					
	Coal Valley (CV)		Tanito Harum (TH)		Malinau (MA)	
Major component						
SiO_2	61.5	(54.8)	57.8	(49.8)	54.6	(46.2)
Al_2O_3	13.9	(21.1)	16.0	(23.4)	15.0	(21.6)
CaO	14.2	(11.9)	9.2	(7.4)	8.0	(6.3)
MgO	3.6	(2.1)	4.8	(2.8)	6.3	(3.6)
FeO	2.2	(2.3)	5.8	(6.0)	7.1	(7.2)
Fe_2O_3	1.4	(3.3)	2.6	(6.0)	3.9	(8.7)
Minor component						
K_2O	1.1	(1.5)	1.4	(1.9)	1.3	(1.8)
TiO_2	0.6	(0.7)	1.0	(1.1)	1.0	(1.1)
P_2O_5	0.1	(0.4)	0.1	(0.4)	0.2	(0.8)
SrO	0.1	(0.2)	0.1	(0.2)	0.1	(0.1)
ZrO_2	0.1	(0.2)	ND[a]	(ND)	0.1	(0.2)
MnO	0.1	(0.1)	0.1	(0.1)	0.1	(0.1)
Cr_2O_3	0.1	(0.2)	ND	(ND)	0.1	(0.2)
BaO	0.2	(0.5)	ND	(ND)	0.1	(0.2)
Na_2O	0.8	(0.7)	1.1	(0.9)	2.1	(1.9)
Total	100.0	(100.0)	100.0	(100.0)	100.0	(100.0)
$\sum[A_2O_3]^b/\sum[RO]^c$	0.76		0.93		0.88	
$[Al_2O_3]/\sum[RO]$	0.69		0.80		0.70	
$[Fe_2O_3]/\sum[RO]$	0.07		0.13		0.18	

$\sum[A_2O_3]/\sum[RO]$: molar ratio of amphoteric and bivalent metal oxides.
[a] Not detected.
[b] A_2O_3: Amphoteric oxide (Al_2O_3, Fe_2O_3).
[c] RO: Bivalent metal oxide (Fe, Ca, Mg, Sr).

Table 2
Chemical composition of synthesized coal slag samples.

Series	Samples	mol% (mass %)										Molar ratio		
		SiO_2		Al_2O_3		CaO		MgO		FeO[a]	Fe_2O_3[a]			
												$\sum[A_2O_3]/\sum[RO]$	$[Al_2O_3]/\sum[RO]$	$[Fe_2O_3]/\sum[RO]$
$(60-x)RO—xA_2O_3—40SiO_2$	CA10.40	40.0 (38.6)		10.0 (16.4)		50.0 (45.0)		0.0 (0.0)		0.0 (0.0)	0.0 (0.0)	0.00	0.20	0.00
	CA20.40	40.0 (35.9)		20.0 (30.5)		40.0 (33.6)		0.0 (0.0)		0.0 (0.0)	0.0 (0.0)	0.00	0.50	0.00
	CA30.40	40.0 (33.6)		30.0 (42.8)		30.0 (23.5)		0.0 (0.0)		0.0 (0.0)	0.0 (0.0)	0.00	1.00	0.00
	CF08.39	39.2 (35.5)		0.0 (0.0)		49.0 (41.4)		0.0 (0.0)		4.0 (4.3)	7.8 (18.8)	0.15	0.00	0.16
	CAF15.11.39	38.6 (30.2)		14.5 (19.3)		29.0 (21.2)		0.0 (0.0)		6.9 (6.5)	11.0 (22.9)	0.71	0.50	0.38
$(50-x)RO—xA_2O_3—50SiO_2$	CA12.50	50.0 (47.1)		12.5 (20.0)		37.5 (33.0)		0.0 (0.0)		0.0 (0.0)	0.0 (0.0)	0.00	0.33	0.00
	CF07.48	48.5 (44.2)		0.0 (0.0)		38.8 (33.0)		0.0 (0.0)		6.1 (6.6)	6.7 (16.2)	0.00	0.00	0.17
$(40-x)RO—xA_2O_3—60SiO_2$	CA00.60	60.0 (61.6)		0.0 (0.0)		40.0 (38.4)		0.0 (0.0)		0.0 (0.0)	0.0 (0.0)	0.00	0.00	0.00
	CA10.60	60.0 (57.2)		10.0 (16.2)		30.0 (26.7)		0.0 (0.0)		0.0 (0.0)	0.0 (0.0)	0.00	0.33	0.00
	MA10.60	60.0 (61.8)		10.0 (17.5)		0.0 (0.0)		30.0 (20.7)		0.0 (0.0)	0.0 (0.0)	0.00	0.33	0.00
	CF02.60	59.5 (59.1)		0.0 (0.0)		37.2 (34.5)		0.0 (0.0)		1.6 (1.9)	1.7 (4.5)	0.04	0.00	0.05
	CF04.59	59.2 (56.9)		0.0 (0.0)		34.5 (30.9)		0.0 (0.0)		2.8 (3.2)	3.5 (8.9)	0.09	0.00	0.10
	CF06.59	58.9 (54.6)		0.0 (0.0)		31.9 (27.6)		0.0 (0.0)		3.8 (4.2)	5.5 (13.6)	0.15	0.00	0.17
	CF07.58	58.3 (52.7)		0.0 (0.0)		29.2 (24.6)		0.0 (0.0)		5.6 (6.1)	6.9 (16.6)	0.20	0.00	0.24
	CF11.58	57.6 (49.1)		0.0 (0.0)		24.0 (19.1)		0.0 (0.0)		7.8 (8.0)	10.5 (23.8)	0.33	0.00	0.44
	CF14.57	57.1 (46.0)		0.0 (0.0)		19.0 (14.3)		0.0 (0.0)		9.8 (9.4)	14.1 (30.2)	0.49	0.00	0.74

[a] The FeO and Fe_2O_3 were determined experimentally using chelate titration method in the quenched samples.

used to discuss their effects on melt density in the results section of this paper.

2.2. Density measurements of slag melts

The apparatus used for the Archimedean double-bob method is similar to apparatus that used in the previous studies [26,43,44], as illustrated in Fig. 1. The principle of this method is to measure the buoyancies of two Pt-bobs with different sizes by using an electrical balance (Sartorius ED124S). A computer interface (Sartorius YCC01-USBM2) was added to monitor and record the buoyancy directly. The measuring temperature was selected for homogeneous melting state. The temperature for homogeneous melting was confirmed by hot thermocouple method [45] and FactSage data bank [46].

The cooled sample was crushed and then re-melted at the highest measuring temperature and was kept for 2 h before density measurements. After the temperature holding, the Pt-bob was suspended by a Pt—Rh 13 wt% wire with 0.25 mm diameter from the bottom of the electrical balance and then Pt-bob was lowered. When the tip of the bob touched the surface of slag melts, the digital balance displayed a change in weight. From the change, it was confirmed that the bob actually had touched the surface of slag melts. Then the bob was lowered further until the bob reached a depth of 20 mm below the surface of the slag melts.

The buoyancies of the large and small bobs were continuously measured for 30 min without removing the bobs from the slag melt in all temperature measurements. The average value of buoyancy was used for density determination. The density of slag melts, ρ, was calculated using the following Eq. (1):

$$\rho = (W_1 - W_2)/(V_1 - V_2) \quad (1)$$

where W_1 and W_2 are the buoyancies, and V_1 and V_2 are the submerged volumes of the large and small bobs, respectively. The thermal expansions of the large and small bobs were corrected by Eq. (2) with the data of the thermal expansion of platinum [47]:

$$V_1 - V_2 = (1 + 3\alpha\Delta T) \cdot (V_1' - V_2') \quad (2)$$

where α is the thermal expansion coefficient of Pt, ΔT is the difference between measuring and room temperatures, and V_1' and V_2' are the volumes of the large and small bobs at room temperature, respectively. The reproducibility of the measurement was evaluated for the densities of silicone fluids and a slag melt of $40Na_2O—60SiO_2$ (mol%) as standard samples.

The density is strongly dependent on the molar weight and the molar volume. The latter is more sensitive to change in structure than density [22]. The molar volume (MV) V_m is calculated using the following Eq. (3):

$$V_m = \sum(x_i \cdot M_i)/\rho \quad (3)$$

where x_i is the molar fraction, and M_i is the molar weight of a component i.

The coefficient of volume expansion (CVE), β, is calculated from the density change corresponding to the temperature measurements by the following Eq. (4):

$$\beta = (\rho_1 - \rho_2)/\rho_2 \cdot 1/(T_2 - T_1) \quad (4)$$

where T_1 is the lowest temperature corresponding to ρ_1, and T_2 is the highest one corresponding to ρ_2.

3. Results and discussion

3.1. Error estimation

The error estimation of the above method was taken as the deviations in the determination of buoyancy, temperature, and electrical balance reading [48]. The individual errors are summarized in Table 3 for each measuring condition. The errors caused by viscosity and inhomogeneity of the sample in density measurements do not exceed $\pm1.5 \times 10^{-2}$ g/cm^3 for CA, $\pm6 \times 10^{-3}$ g/cm^3 for CF, $\pm2 \times 10^{-3}$ g/cm^3 for CAF, and $\pm5.2 \times 10^{-2}$ g/cm^3 for MA synthesized slags, $\pm1.2 \times 10^{-2}$ g/cm^3 for gasified coal slags. The error range was depended on composition in slag melts. The average value of error was 0.37% for all measured densities.

The accuracy of density measurements was determined in the following ways. Firstly, the densities of silicone fluids with the viscosities 0.01, 0.999, 4.850, and 29.44 Pa s were measured at 25 °C. The densities of silicone fluids were tested to be 0.941, 0.972, 0.973, and 0.974 g/cm^3, respectively. The measured densities have good agreement with the data of silicone fluid standards [49] with a precision of 0.16%. Secondly, the density of $40Na_2O—60SiO_2$ (mol %) melt was measured at 1350–1500 °C. The density results of $40Na_2O—60SiO_2$ melts are shown in Fig. 2. The results show that the mean difference between the first and second measurements is within 0.61% of the density values. The reproducibility of this

Table 3
Properties related density of gasified coal and synthesized slag melts.

Samples	Fe^{3+}/Fe_{tot}[a]	Density[b], at temperature (°C)										Molar volume[b]						β[b]
		1350		1400		1450		1500		1550		1600		1350	1400	1450	1500	1550	1600	
CA10.40	–	2.696	(0.002)[c]	2.676	(0.003)	2.675	(0.002)	2.657	(0.003)	2.637	(0.005)	–		23.1	23.3	23.3	23.4	23.6	–	11.2
CA20.40	–	–		2.665	(0.003)	2.639	(0.002)	2.625	(0.003)	2.603	(0.003)	–		–	25.1	25.3	25.5	25.7	–	15.7
CA30.40	–	–		–		–		2.597	(0.005)	2.571	(0.004)	–		–	–	–	27.5	27.8	–	20.4
CF08.39	0.80	2.972	(0.005)	2.964	(0.002)	2.943	(0.002)	2.929	(0.005)	2.918	(0.006)	–		22.3	22.4	22.5	22.7	22.7	–	9.3
CAF15.11.39	0.76	–		3.012	(0.001)	2.998	(0.001)	2.992	(0.002)	2.967	(0.002)	–		–	20.6	20.7	20.7	20.9	–	10.0
CA12.50	–	2.607	(0.006)	2.594	(0.005)	2.563	(0.006)	2.546	(0.007)	2.535	(0.004)	–		24.5	24.6	24.9	25.1	25.2	–	14.2
CF07.48	0.69	2.953	(0.002)	2.931	(0.001)	2.913	(0.001)	2.902	(0.001)	2.879	(0.001)	–		22.3	22.5	22.6	22.7	22.9	–	12.9
CA00.60	–	–		–		2.540	(0.003)	2.525	(0.003)	2.508	(0.002)	–		–	–	23.0	23.2	23.3	–	13.5
CA10.60	–	2.54	(0.02)	2.515	(0.007)	2.495	(0.005)	2.491	(0.003)	2.479	(0.004)	–		24.9	25.1	25.3	25.3	25.5	–	11.4
MA10.60	–	–		–		2.48	(0.05)	2.47	(0.01)	2.453	(0.005)	–		–	–	23.5	23.6	23.8	–	10.6
CF02.60	0.68	–		–		2.589	(0.001)	2.577	(0.001)	2.564	(0.002)	–		–	–	23.4	23.5	23.6	–	9.7
CF04.59	0.72	–		2.677	(0.001)	2.667	(0.002)	2.656	(0.001)	2.644	(0.001)	–		–	23.4	23.4	23.6	23.7	–	8.3
CF06.59	0.75	2.751	(0.002)	2.743	(0.001)	2.731	(0.002)	2.718	(0.001)	2.709	(0.001)	–		23.5	23.6	23.7	23.8	23.9	–	8.2
CF07.58	0.71	2.835	(0.001)	2.826	(0.002)	2.805	(0.001)	2.799	(0.001)	2.793	(0.002)	–		23.5	23.5	23.7	23.7	23.8	–	7.4
CF11.58	0.73	2.930	(0.002)	2.924	(0.001)	2.908	(0.001)	2.893	(0.001)	2.885	(0.002)	–		24.1	24.1	24.2	24.4	24.4	–	7.8
CF14.57	0.74	–		–		3.032	(0.003)	3.019	(0.003)	3.002	(0.004)	–		–	–	24.6	24.7	24.8	–	10.1
CV	0.56	–		–		–		–	–	2.53	(0.01)	2.513	(0.007)	–	–	–	–	26.7	26.8	12.2
TH	0.47	–		–		–		2.566	(0.003)	2.548	(0.003)	2.535	(0.002)	–	–	–	27.2	27.4	27.5	10.4
MA	0.52	–		–		–		2.570	(0.003)	2.559	(0.002)	2.541	(0.001)	–	–	–	27.6	27.7	27.9	14.1

[a] The fraction of Fe^{3+}/Fe_{tot} was analyzed two or three times for quenched samples.
[b] The units of density, molar volume, and coefficient of volume expansion (β) are g/cm^3, cm^3/mol and $10^{-5}/K$, respectively.
[c] The number in brackets represent individual error's estimation for each temperature and composition.

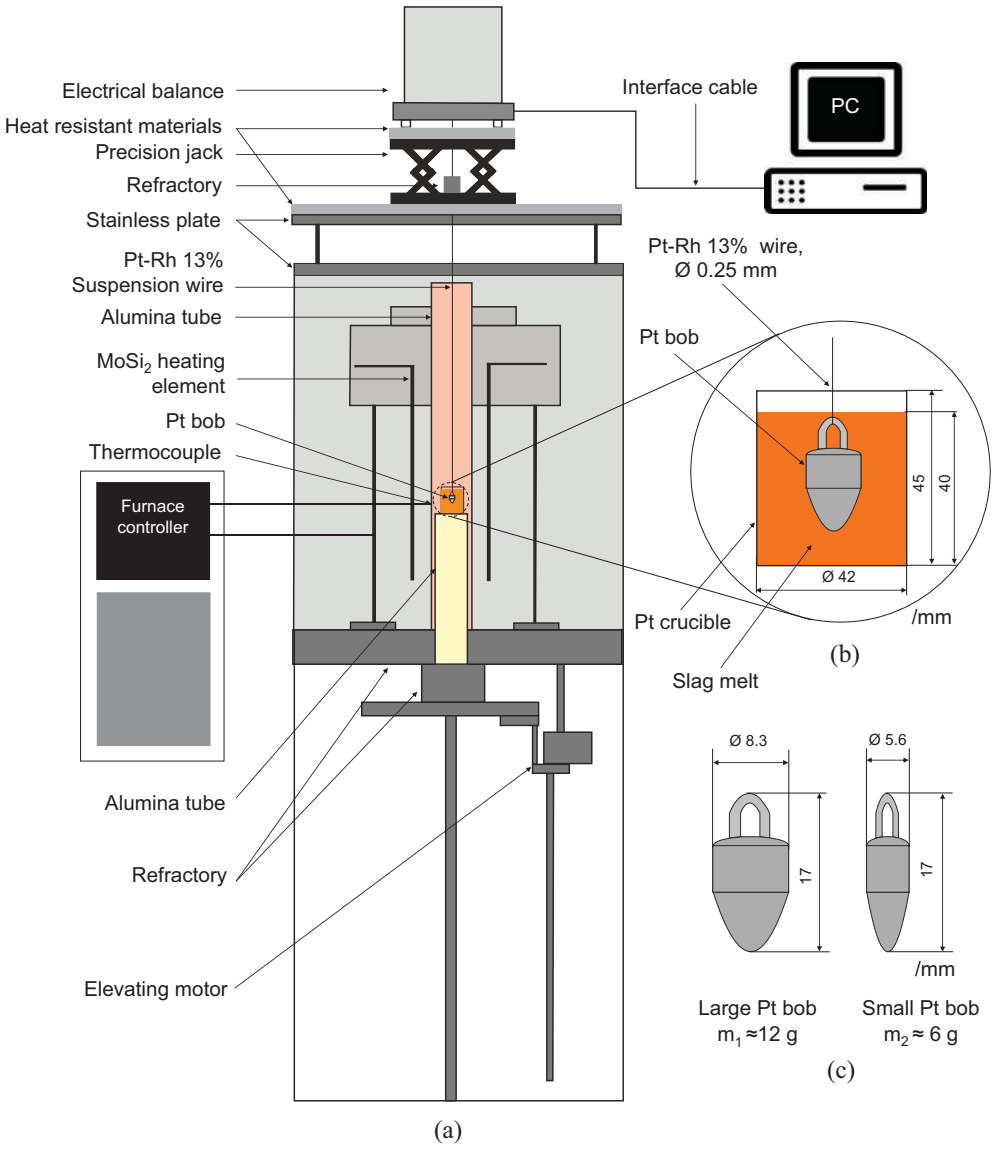

Fig. 1. Schematic apparatus for density measurements of slag melts: (a) whole diagram, (b) sample, and (c) large and small bobs.

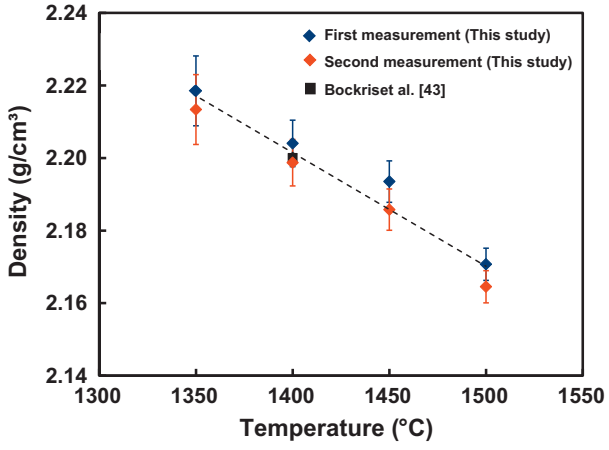

Fig. 2. Variation of density with temperature for $40Na_2O$—$60SiO_2$ slag melt (mol%) with the previously reported value Bockris et al. [43]. The dashed line represents the average linear fit of densities measured in this study.

work is within the error estimation of density measurements. Furthermore, the density values are good agreement with previously reported values [43] within a deviation of 0.10%. The accuracy and reproducibility of density for silicone fluids and the $40Na_2O$—$60SiO_2$ (mol%) melt support the reasonable results of density measurements.

3.2. Density measurements

Table 3 summarizes the results of density, MV and CVE for gasified coal and synthesized slag melts. Table 3 also gives the analyzed values of Fe^{3+}/Fe_{tot} in quenched samples. The experiments were conducted two or three times for each sample. The experimental results showed that the percentage of Fe^{3+} was accounted for 47–56% and 68–80% for gasified and synthesized quenched samples, respectively. A close agreement is found by data of previous study with the similar compositions with the Fe^{3+} percentage of 45–90% [35].

Fig. 3 shows the temperature dependences of density for coal slag melts. There are linear relationships between density and temperature for all coal slag melts between 1500 and 1600 °C. The

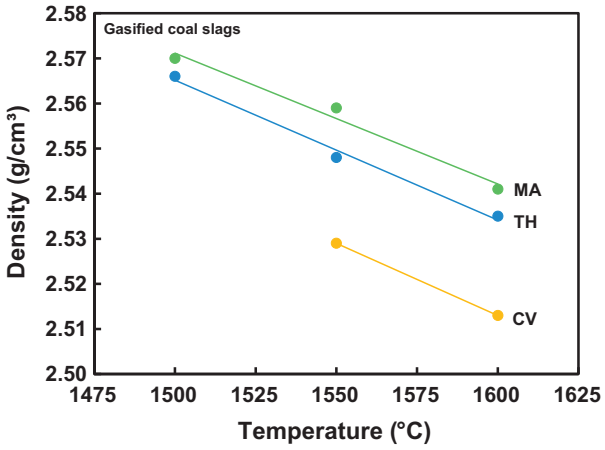

Fig. 3. Variations of density with temperature for coal slag melts. The straight lines are least square fit to the data of the coal slag melts at measuring temperatures.

densities of the coal slag melts decrease linearly with increasing temperature. The density varied from 2.513 to 2.570 g/cm^3. The density was found to increase in the order of CV < TH < MA with increasing Fe_2O_3 and FeO contents, as shown in Table 1. In addition, the density decreases with increasing Al_2O_3 and SiO_2 contents.

Figs. 4 and 5 show the temperature dependences of density for synthesized slag melts with various Al_2O_3 and Fe_2O_3 contents. The density decreases linearly with increasing temperature as a general trend in slag melts [22]. The slag melt containing the largest Fe_2O_3 concentration of 14 mol%, named as CF14.57, has larger density values, compared to all the other samples at 1350–1550 °C. The density monotonically decreases when Fe_2O_3 is replaced by Al_2O_3 for synthesized slag melts with constant SiO_2 contents (40, 50, and 60 mol%), as shown in Table 3 and Figs. 4 and 5. The density is also found to decrease as Al_2O_3 content increases in the range of 10 and 30 mol%. The density of 30CaO—10Al_2O_3—60SiO_2 (CA10.60) slag melt is slightly bigger than that of 30MgO—10Al_2O_3—60SiO_2 (MA10.60) sample due to the substitution of CaO for MgO.

Densities of gasified and synthesized coal slag melts are shown in Figs. 3–5 and are summarized in Table 3. The densities of CAS and CFS slag melts show different trends with respect to increase in Al_2O_3 and Fe_2O_3 contents. The density of slag melts decreases

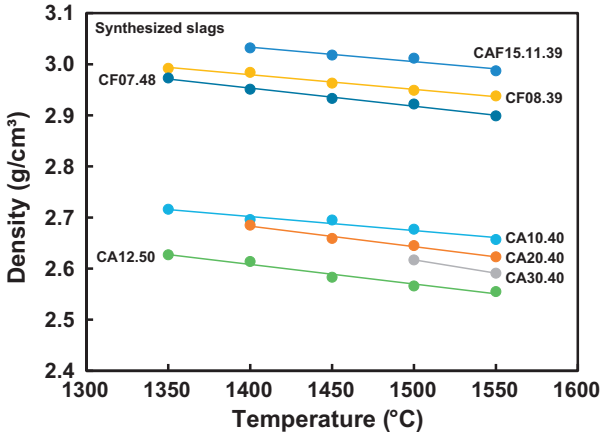

Fig. 4. Variations of density with temperature in a series of (60 – x)RO—xA_2O_3—40SiO_2 and (50 – x) RO—xA_2O_3—50SiO_2 slag melts (Table 2) with various Al_2O_3 and Fe_2O_3 contents. The straight lines are least square fit to the data of the synthesized slag melts at measuring temperatures.

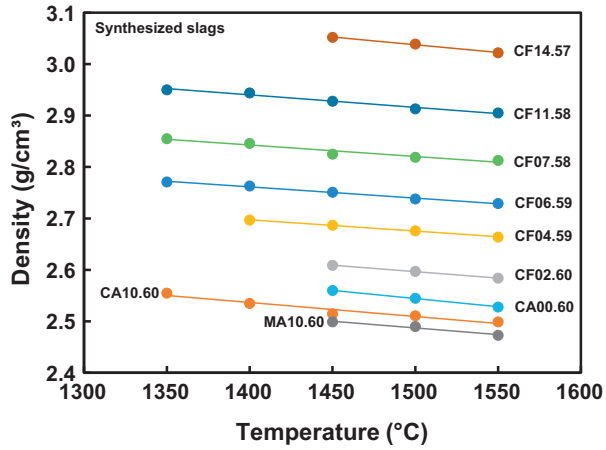

Fig. 5. Variations of density with temperature in a series of (40 – x)RO—xAl_2O_3—60SiO_2 slag melts (Table 2) with various Al_2O_3 and Fe_2O_3 contents. The lines are the same as those in Fig. 4.

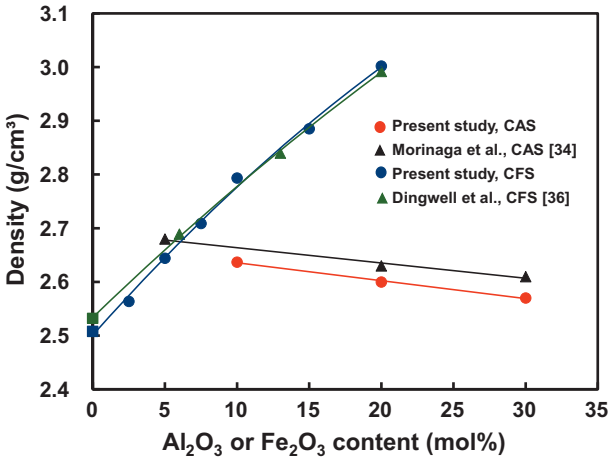

Fig. 6. Variation of density with Al_2O_3 or Fe_2O_3 content in a series of (60 – x) CaO—xAl_2O_3—40SiO_2 (CAS) and (40 – x)CaO—xFe_2O_3—60SiO_2 (CFS) slag melts (Table 2) at 1550 °C, respectively. Solid circles (red and blue) are the results of present studies. Solid triangles (black and green) are reported values by Morinaga et al. [34] and Dingwell et al. [36]. Solid squares (blue and green) are binary slag melts of 40CaO—60SiO_2. The solid lines of CAS and CFS are least square and polynomial fits to the data, respectively. (For interpretation of the references to color in this figure legend, the reader is referred to the web version of this article.)

almost monotonically with increasing Al_2O_3 content and increases with increasing Fe_2O_3 content.

Fig. 6 shows the relationship between density and A_2O_3 content (A = Al or Fe) for slag melts of CAS with 40 mol% SiO_2 and CFS with 60 mol% SiO_2. The densities shown in Fig. 6 are the measured values at 1550 °C. A comparison between our results and reported values in the CAS slag melts shows slight deviation [34] and has a good agreement in the CFS slag melts [36].

3.3. Molar volume

The molar volumes of synthesized slag melts with various Al_2O_3 and Fe_2O_3 contents are shown in Figs. 7 and 8. Fig. 7 shows the relationship between molar volume (MV) and Al_2O_3 content in a series of CAS slag melts with 40 mol% SiO_2. MVs of the slag melts at 1400–1550 °C increase monotonically with increasing Al_2O_3 content. MVs of CAS slag melts are in the range of 23.6–27.8 cm^3/mol (Table 3). A good agreement of MV is found with data of CAS slag melts with similar compositions [34]. MV increases with increasing

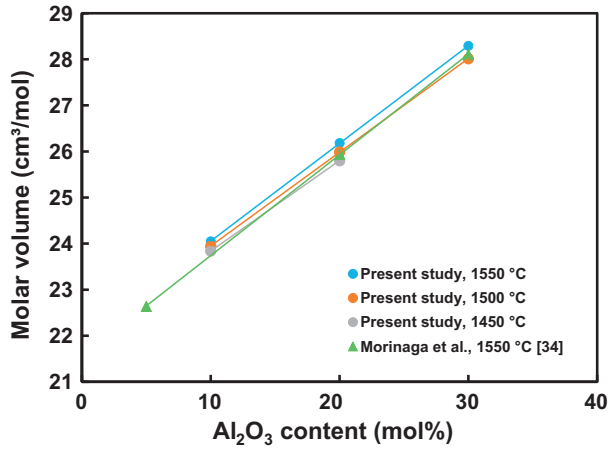

Fig. 7. Variations of molar volume with Al_2O_3 content in a series $(60 - x)CaO—xAl_2O_3—40SiO_2$ slag melts (Table 2). Solid triangles (green) are reported values by Morinaga et al. [34]. The lines are the same as those in Fig. 4. (For interpretation of the references to color in this figure legend, the reader is referred to the web version of this article.)

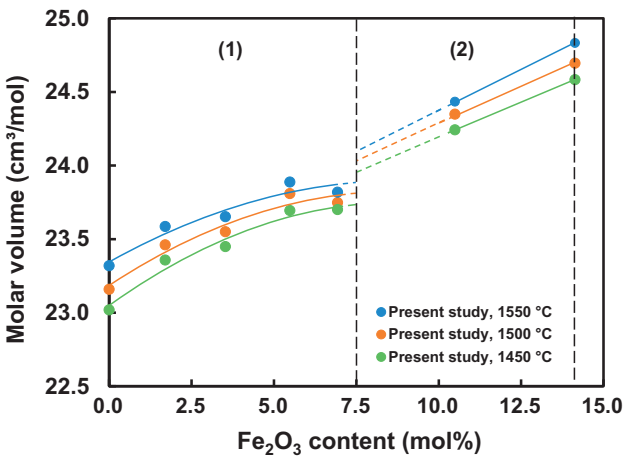

Fig. 8. Variations of molar volume with Fe_2O_3 content in a series of $(40 - x)CaO—xFe_2O_3—60SiO_2$ slag melts (Table 2). Solid and dashed lines represent the experimental results and the guide lines to eyes at the boundary between regions (1) and (2), respectively. The molar volume using polynomial fits reaches constant values at ~7.5 mol% Fe_2O_3 in the region (1). The molar volume using least square fits exhibits discontinuously change between the regions (1) and (2).

Fe_2O_3 content in a series of CFS slag melts with 60 mol% SiO_2, as shown in Fig. 8. The composition dependence of MV in the CFS series seems to be classified into two regions as (1) $0 \leqslant x \leqslant 7.5$ and (2) $7.5 \leqslant x \leqslant 14$ due to discontinuous change. MVs of CFS slag melts are in the range of 23–24.8 cm^3/mol (Table 3). MV reaches almost constant values at ~7.5 mol% Fe_2O_3.

MV tends to increase by adding Al_2O_3 and Fe_2O_3 in the $CaO—SiO_2$ slag melts. Hence, MV of CAS slag melts monotonically increases (Fig. 7), however, MV of CFS slag melts has the discontinuous change at the boundary between the regions (1) and (2) (Fig. 8). This change suggests that the structural change of CFS slag melts occurred at $\geqslant$7.5 mol% Fe_2O_3.

3.4. Coefficient of volume expansion

Fig. 9 shows the relationship between the coefficient of volume expansion (CVE) and Al_2O_3 content for CAS slag melts. CVE increases monotonically with increasing Al_2O_3 content. Fig. 10 shows the variation of CVE with Fe_2O_3 content for CFS slag melts. CVE of slag melts exhibits in the range of 7.4–13.5 $\times 10^{-5}$/K

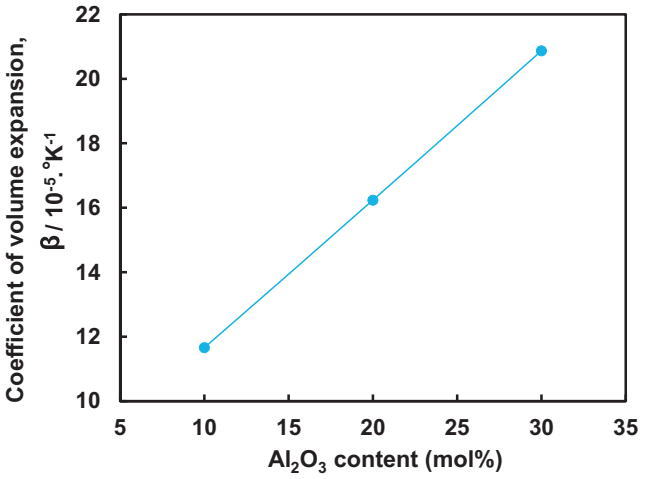

Fig. 9. Variation of the coefficient of volume expansion with Al_2O_3 content in a series of $(60 - x)$ $CaO—xAl_2O_3—40SiO_2$ slag melts (Table 2). The line is the same as those in Fig. 4.

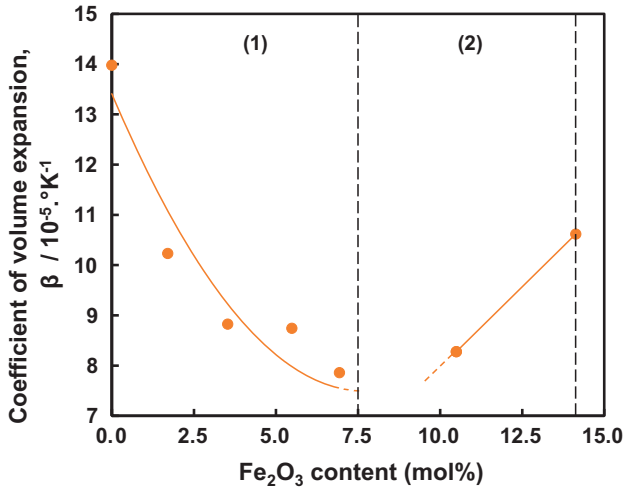

Fig. 10. Variation of the coefficient of volume expansion with Fe_2O_3 content in a series of $(40 - x)CaO—xFe_2O_3—60SiO_2$ slag melts (Table 2). The solid and dashed lines are the same as those in Fig. 8.

(Table 3). CVE is also classified into the two regions (1) and (2). CVE decreased with Fe_2O_3 addition exhibiting a minimum value at ~7 mol% and increased in region (2) of $x \geqslant 7.5$. The trend of CVE corresponds to that of the molar volume (Fig. 9).

Since CVE is calculated from the measured densities at various temperatures. It corresponds to the change of density with temperature. The minimum of CVE suggests that the temperature-induced structural change of the CFS slag melts occurs at ~7 mol% Fe_2O_3.

The density of CAS melt samples with $\geqslant$10 mol% Al_2O_3 has not been measured because of high temperature for homogenous melting, e.g., the CA00.40 at 1625 °C [46]. The good density results were obtained without solid components in the CAS slag melts.

3.5. The influence of Al_2O_3 and Fe_2O_3 on density

It is well known that Al_2O_3 and Fe_2O_3 are amphoteric oxides and their influence depends on the type and content of NWM as the basicity of slag melts [5,14,34]. The addition of CaO results in breaking the structure of silicate network and decreasing melt viscosity substantially. Influence of Al_2O_3 addition depends on $[Al_2O_3]/[R_2O, R'O]$ in molar ratio due to simple stoichiometric consideration. In the case of the molar ratio $[Al_2O_3]/[RO] < 1$, Al_2O_3

behaves NWF as described in previous studies of alumino-silicate melts and glasses [5,34,40]. Several authors reported that viscosity increased with increasing the polymerization degree of network structure by Al_2O_3 addition [34,50]. In other words, Al^{3+} ideally plays the role of NWF for AlO_4 formation in order to link and share the corner between AlO_4 tetrahedra when charge compensating cation such as CaO exists enough for Al at $[Al_2O_3]/[CaO] \leqslant 1$ [14,33,40]. Moreover, the addition of Al_2O_3 to CaO—SiO_2 melts due to the formation of AlO_4 tetrahedral corresponds to the increases of MV and CVE [34].

The influences of CaO, MgO, and FeO contents as basic oxide (NWM) on density of synthesized slag melts are shown in Fig. 5 and Table 3. The influence of CaO on density in CAS and CFS systems depends on molar ratio of $[Al_2O_3]/[CaO]$ and $[Fe_2O_3]/[CaO]$. Density of CAS system decreases with increasing molar ratio of $[Al_2O_3]/[CaO]$ for 40 mol% SiO_2, as shown in Tables 2 and 3. On the contrary, the density increases with increasing molar ratio of $[Fe_2O_3]/[CaO]$ for ~60 mol% SiO_2 in CFS system. Similarly, the influence of FeO on density in CFS system increases with increasing FeO content, as shown in Table 3. Meanwhile, the influence of MgO on density of slag melts was investigated by substituting of CaO in CA10.60 sample by MgO (MA10.60). The result shows that MgO has little effect on density of slag melts, as shown in Fig. 5. This result corresponds well with previous studies [37,51].

In order to obtain the influence of Fe_2O_3 on the structure of slag melts, the molar volume (MV) and the coefficient of volume expansion (CVE) are used to support our discussion, as shown in Figs. 8 and 10. MV exhibits the discontinuous change at ~7.5 mol% Fe_2O_3 (x). This boundary corresponds well to the two regions of CVE with $0 \leqslant x \leqslant 7.5$ and $7.5 \leqslant x \leqslant 14$ mol% Fe_2O_3.

In the region (1) of CFS slag melts, MV tends to increase by adding Fe_2O_3 and reaches constant values at ~7.5 mol% Fe_2O_3. These results correspond to the decreasing of CVE in the region (1), and it passes through a minimum at ~7 mol% Fe_2O_3, and then increases again in the region (2). Previous study [35] reported that the oxygen coordination number of Fe^{3+} ions can be determined by the ratio $[Fe_2O_3]/[R_2O, R'O]$. In the similar compositions of CFS quenched slag samples, Fe^{3+} as NWF and NWM are favored at $Fe_2O_3 \leqslant 10$ mol% and 10–20 mol%, respectively [35,52]. It is suggested that the larger Fe_2O_3 content of >10 mol% may form inhomogeneous melt structure including small crystals even in melt state. Further studies are necessary to be done in order to understand the structure of silicate melts including large amounts of Fe_2O_3 (>10 mol%).

3.6. Composition parameter

The contribution of main components of SiO_2, Al_2O_3, CaO, MgO, FeO and Fe_2O_3 on density was investigated for coal and synthesized slag melts. It was found experimentally that main components have different contributions on the density and molar volume of slag melts. Based on measured density data of slag melts, a composition parameter is proposed to predict densities from the corresponding components determined by Eq. (5):

$$P_\rho = 2.18 \cdot f_{SiO_2} + 2.73 \cdot f_{Al_2O_3} + 2.96 \cdot f_{CaO} + 2.92 \cdot f_{MgO} + 4.88 \cdot f_{FeO} + 5.00 f_{Fe_2O_3} \quad (5)$$

where P_ρ is composition parameter of density, and f is the fraction of each component expressed by mol%.

Fig. 11 shows the relationship between density and the composition parameter for the density values measured at 1550 °C. It compares with experimental and calculated results using the composition parameter for all density data. The average error Δ of all calculated values can be evaluated by using Eqs. (6) and (7):

$$\delta_n = (\rho_n)_{cal} - (\rho_n)_{mea}/(\rho_n)_{mea} \cdot 100\ (\%) \quad (6)$$

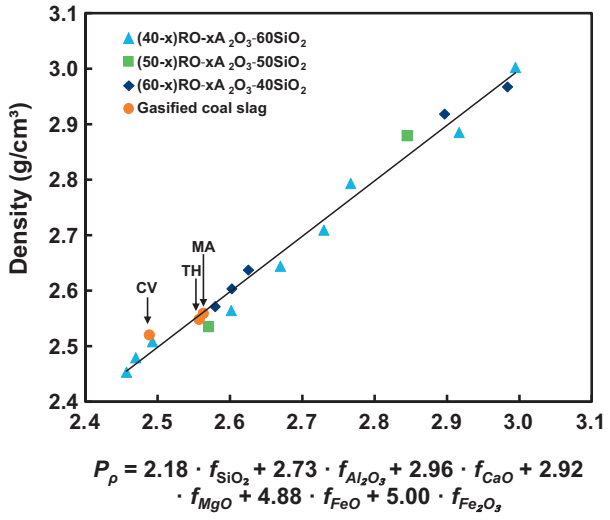

Fig. 11. Variation of density with the composition parameter based on mole percentage for synthesized and coal slag melts at 1550 °C.

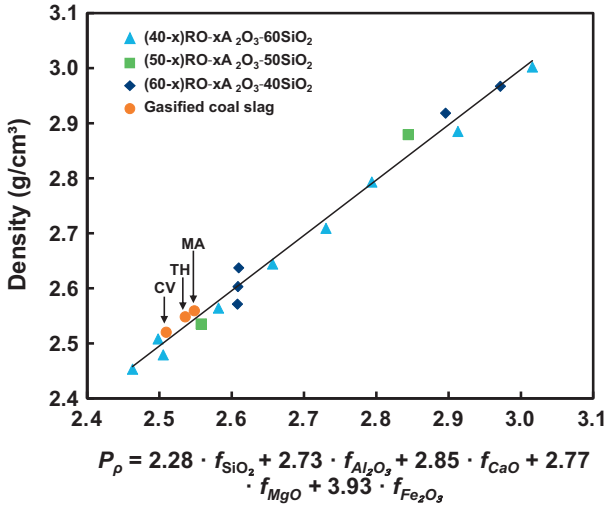

Fig. 12. Variation of density with the composition parameter based on mass percentage for synthesized and coal slag melts at 1550 °C, without considering valence state of iron.

$$\Delta = \frac{1}{N}\sum_{n=1}^{N}|\delta_n|\ (\%) \quad (7)$$

where δ_n is the percentage difference between the calculated $(\rho_n)_{cal}$ and measured $(\rho_n)_{mea}$ density values, and Δ is calculated by taking the summation sign $\sum$ of all absolute values of δ_n and divided by the total number of data.

The calculated value of the average error is 0.69%, which indicates a strong positive correlation between measured density and composition parameter for gasified and synthesized slag melts. This new model has the capability to predict the density of slag melts based on mole percentage.

For engineering application, the composition parameter is used for predictions of the densities using mass percentage of synthesized coal slags as shown in Fig. 12. Because of generally low contents of FeO (⩽10 mol%) in the investigated valence states of iron oxides, the contributions of the densities due to FeO were neglected and assumed that all of Fe component was Fe_2O_3. Based on these considerations, the second composition parameter as shown in Eq. (8) is used,

$$P_\rho = 2.28 \cdot f_{SiO_2} + 2.73 \cdot f_{Al_2O_3} + 2.85 \cdot f_{CaO} + 2.77 \cdot f_{MgO} + 3.93 f_{Fe_2O_3} \quad (8)$$

The second composition parameter can be used to estimate the densities of gasified coal slag melts as a function of composition mass % and confirmed that the calculated value of the average error was 0.66%. Furthermore, the empirical composition parameter can be beneficially used to predict density of gasified coal slag melts by the analysis of their chemical compositions without density measurements.

4. Conclusions

The density of the gasified coal slags collected from the next-generation IGCC pilot plant and synthesized slag melts was measured using the Archimedean double-bob method in the temperature range of 1350 and 1600 °C. The MV and the CVE were calculated using measured density. Sixteen different synthesized slag compositions were chosen based on the main components of the gasified coal slags: SiO_2, Al_2O_3, CaO, MgO, FeO and Fe_2O_3. The results obtained are summarized below:

1. Density of slag melts decreased linearly with increasing temperature for all samples.
2. Densities of gasified coal slag melts were found to increase in the order of CV < TH < MA. The density decreased with increasing Al_2O_3 and SiO_2 contents, on the contrary, it increased with increasing Fe_2O_3 and FeO contents.
3. Two types of amphoteric oxide in slag melts brought about different effects on the density: the density decreased with increasing Al_2O_3 content, on the contrary, it increased with increasing Fe_2O_3 content.
4. The MV and the CVE monotonically increased with increasing Al_2O_3 content for CaO—Al_2O_3—SiO_2 slag melts.
5. On the basis of the MV and CVE, their composition variations with Fe_2O_3 content were classified into two regions: (1) low concentration ($0 \leqslant x \leqslant 7.5$) and (2) high concentration ($7.5 \leqslant x \leqslant 14$). The MV increases with increasing Fe_2O_3 content with the discontinuous change between the boundary of the two regions ($x \sim 7.5$ mol%). The trend of the CVE corresponds to the MV. The CVE decreased with Fe_2O_3 addition showing a minimum value at ~7 mol% Fe_2O_3 and increased in $7.5 \leqslant x \leqslant 14$ mol% Fe_2O_3.
6. An empirical composition parameter was proposed to predict the density from the corresponding chemical composition of gasified coal slag melts for the next-generation IGCC.

Acknowledgements

This research is supported by New Energy and Industrial Technology Development Organization (NEDO) of Japan. The first author is sponsored to pursue a doctoral degree at Ehime University by Directorate General of Human Resource for Science, Technology and Higher Education, Indonesia. The authors thank to Dr. Lukmanul Hakim Arma for his critical reading on our manuscript.

References

[1] Mondol JD, McIlveen-Wright D, Rezvani S, Huang Y, Hewitt N. Techno-economic evaluation of advanced IGCC lignite coal fuelled power plants with CO_2 capture. Fuel 2009;88:2495–506. http://dx.doi.org/10.1016/j.fuel.2009.04.019.
[2] Franco A, Diaz AR. The future challenges for "clean coal technologies": joining efficiency increase and pollutant emission control. Energy 2009;34:348–54. http://dx.doi.org/10.1016/j.energy.2008.09.012.
[3] Cau G, Tola V, Deiana P. Comparative performance assessment of USC and IGCC power plants integrated with CO_2 capture systems. Fuel 2014;116:820–33. http://dx.doi.org/10.1016/j.fuel.2013.06.005.
[4] Oki Y, Hara S, Umemoto S, Kidoguchi K, Hamada H, Kobayashi M, et al. Development of high-efficiency oxy-fuel IGCC system. Energy Proc 2014;63:471–5. http://dx.doi.org/10.1016/j.egypro.2014.11.050.
[5] Takebe H, Tsuruda A, Okada A, Ueda K. Viscosity characteristic of molten slag for next-generation IGCC. J Jpn Inst Energy 2015;94(5):450–4.
[6] Minchener AJ. Coal gasification for advanced power generation. Fuel 2005;84:2222–35. http://dx.doi.org/10.1016/j.fuel.2005.08.035.
[7] Kong L, Bai J, Li W, Wen X, Li X, Bai Z, et al. The internal and external factor on coal ash slag viscosity at high temperatures, Part 1: Effect of cooling rate on slag viscosity, measured continuously. Fuel 2015;158:968–75. http://dx.doi.org/10.1016/j.fuel.2015.02.055.
[8] Kong L, Bai J, Li W, Wen X, Liu X, Li X, et al. The internal and external factor on coal ash slag viscosity at high temperatures, Part 2: Effect of residual carbon on slag viscosity. Fuel 2015;158:976–82. http://dx.doi.org/10.1016/j.fuel.2015.06.055.
[9] Strezov V, Lucas JA, Wall TF. Effect of pressure on the swelling of density separated coal particles. Fuel 2005;84:1238–45. http://dx.doi.org/10.1016/j.fuel.2004.06.035.
[10] Aineto M, Acosta A, Rincón JM, Romero M. Thermal expansion of slag and fly ash from coal gasification in IGCC power plant. Fuel 2006;85:2352–8. http://dx.doi.org/10.1016/j.fuel.2006.05.015.
[11] Shannon GN, Matsuura H, Rozelle P, Fruehan RJ, Pisupati S, Sridhar S. Effect of size and density on the thermodynamic predictions of coal particle phase formation during coal gasification. Fuel Process Technol 2009;90:1114–21. http://dx.doi.org/10.1016/j.fuproc.2009.05.002.
[12] Lin X, Ideta K, Miyawaki J, Takebe H, Yoon SH, Mochida I. A Study on the correlation of structure and fluidity of three Asian coal ashes and slags. J Nov Carbon Resour Sci 2012;5:5–9.
[13] Lin X, Ideta K, Miyawaki J, Takebe H, Yoon SH, Mochida I. Correlation between fluidity properties and local structures of three typical Asian coal ashes. Energy Fuels 2012;26:2136–44. http://dx.doi.org/10.1021/ef201771f.
[14] Mills KC, Yuan L, Jones RT. Estimating the physical properties of slags. J S Afr Inst Min Metall 2011;111:649–58.
[15] Jiang Y, Lin X, Ideta K, Takebe H, Miyawaki J, Yoon SH, et al. Microstructural transformations of two representative slags at high temperatures and effects on the viscosity. J Ind Eng Chem 2014;20:1338–45. http://dx.doi.org/10.1016/j.jiec.2013.07.015.
[16] Hsieh PY, Kwong KS, Bennett J. Correlation between the critical viscosity and ash fusion temperatures of coal gasifier ashes. Fuel Process Technol 2016;142:13–26. http://dx.doi.org/10.1016/j.fuproc.2015.09.019.
[17] Kondratiev A, Jak E. Predicting coal ash slag flow characteristics (viscosity model for the Al_2O_3–CaO–"FeO"–SiO_2 system). Fuel 2001;80:1989–2000. http://dx.doi.org/10.1016/S0016-2361(01)00083-7.
[18] Van Dyk JC, Waanders FB, Benson SA, Laumb ML, Hack K. Viscosity predictions of the slag composition of gasified coal, utilizing FactSage equilibrium modelling. Fuel 2009;88:67–74. http://dx.doi.org/10.1016/j.fuel.2008.07.034.
[19] Ye I, Ryu C. Numerical modeling of slag flow and heat transfer on the wall of a coal gasifier. Fuel 2015;150:64–74. http://dx.doi.org/10.1016/j.fuel.2015.01.111.
[20] Mysen BO, Virgo D, Seifert FA. The structure of silicate melts: implications for chemical and physical properties of natural magma. Rev Geophys Sp Phys 1982;20:353–83. http://dx.doi.org/10.1029/RG020i003p00353.
[21] Mills KC. Estimation of physicochemical properties of coal slag and ashes. Miner Mater Ash Coal, Am Chem Soc Washington, DC 1986;301:195–214. http://dx.doi.org/10.1021/bk-1986-0301.ch015.
[22] Hwang C, Fujino S, Morinaga K. Density of Bi_2O_3–B_2O_3 binary melts. J Am Ceram Soc 2004;87:1677–82. http://dx.doi.org/10.1111/j.1551-2916.2004.01677.x.
[23] Kuromitsu Y, Yoshida H, Takebe H, Morinaga K. Interaction between alumina and binary glasses. J Am Ceram Soc 1997;80(6):1583–7. http://dx.doi.org/10.1111/j.1151-2916.1997.tb03020.x.
[24] Toyoda S, Fujino S, Morinaga K. Density, viscosity and surface tension of 50RO–$50P_2O_5$ (R: Mg, Ca, Sr, Ba, and Zn) glass melts. J Non Cryst Solids 2003;321:169–74. http://dx.doi.org/10.1016/S0022-3093(03)00174-1.
[25] Shartsis L, Spinner S, Capps W. Density, expansivity, and viscosity of molten alkali silicates. J Am Ceram Soc 1952;35:155–60. http://dx.doi.org/10.1111/j.1151-2916.1952.tb13090.x.
[26] Dingwell DB, Brearley M, Dickinson JE. Melt densities in the Na_2O–FeO–Fe_2O_3–SiO_2 system and the partial molar volume of tetrahedrally-coordinated ferric iron in silicate melts. Geochim Cosmochim Acta 1988;52:2467–75. http://dx.doi.org/10.1016/0016-7037(88)90305-5.
[27] Muhmood L, Seetharaman S. Density measurements of low silica CaO–SiO_2–Al_2O_3 slags. Metall Mater Trans B 2010;41:833–40. http://dx.doi.org/10.1007/s11663-010-9385-1.
[28] Lee J, Hoai LT, Choe J, Park JH. Density measurements of CaO–MnO–SiO_2 slags. ISIJ Int 2012;52:2145–8. http://dx.doi.org/10.2355/isijinternational.52.2145.
[29] Sugawara T, Katsuki J, Shiono T, Yoshida S, Matsuoka J, Minami K, et al. High-temperature heat capacity and density of simulated high-level waste glass. J Nucl Mater 2014;454:298–307. http://dx.doi.org/10.1016/j.jnucmat.2014.07.055.
[30] Linard Y, Nonnet H, Advocat T. Physicochemical model for predicting molten glass density. J Non Cryst Solids 2008;354:4917–26. http://dx.doi.org/10.1016/j.jnoncrysol.2008.07.013.

[31] Mills KC. The influence of structure on the physico-chemical properties of slags. ISIJ Int 1993;33:148–55. http://dx.doi.org/10.2355/isijinternational.33.148.
[32] Xuan W, Whitty KJ, Guan Q, Bi D, Zhan Z, Zhang J. Influence of SiO_2/Al_2O_3 on crystallization characteristics of synthetic coal slags. Fuel 2015;144:103–10. http://dx.doi.org/10.1016/j.fuel.2014.11.091.
[33] Aksay I, Pask J, Davis R. Densities of SiO_2–Al_2O_3 melts. J Am Ceram Soc 1973;62 (7–8):332–6. http://dx.doi.org/10.1111/j.1151-2916.1979.tb19071.x.
[34] Morinaga K, Suginohara Y, Yanagase T. Density of CaO–SiO_2–Fe_2O_3, –Al_2O_3 melts. Tech Rep Kyushu Univ 1975;48(6):859–65.
[35] Morinaga K, Suginohara Y, Yanagase T. Oxygen coordination number of Fe ions in CaO–SiO_2 and Na_2O–SiO_2 systems. J Jpn Inst Met Mater 1976;40(05):480–6.
[36] Dingwell DB, Brearley M. Melt densities in the CaO–FeO–Fe_2O_3–SiO_2 system and the compositional dependence of the partial molar volume of ferric iron in silicate melts. Geochim Cosmochim Acta 1988;52:2815–25. http://dx.doi.org/10.1016/0016-7037(88)90149-4.
[37] Courtial P, Dingwell DB. Nonlinear composition dependence of molar volume of melts in the CaO–Al_2O_3–SiO_2 system. Geochim Cosmochim Acta 1995;59 (18):3685–95. http://dx.doi.org/10.1016/0016-7037(95)00272-2.
[38] Neuville DR, Cormier L, Massiot D. Al coordination and speciation in calcium aluminosilicate glasses: effects of composition determined by 27Al MQ-MAS NMR and Raman spectroscopy. Chem Geol 2006;229:173–85. http://dx.doi.org/10.1016/j.chemgeo.2006.01.019.
[39] Chevrel MO, Giordano D, Potuzak M, Courtial P, Dingwell DB. Physical properties of $CaAl_2Si_2O_8$–$CaMgSi_2O_6$–FeO–Fe_2O_3 melts: analogues for extra-terrestrial basalt. Chem Geol 2013;346:93–105. http://dx.doi.org/10.1016/j.chemgeo.2012.09.004.
[40] Takahashi S, Neuville DR, Takebe H. Thermal properties, density and structure of percalcic and peraluminus CaO–Al_2O_3–SiO_2 glasses. J Non Cryst Solids 2015;411:5–12. http://dx.doi.org/10.1016/j.jnoncrysol.2014.12.019.
[41] Nakashima K, Saito N, Sukenaga S. Viscosity of iron oxide containing slag. J MMIJ 2011;127:111–6. http://dx.doi.org/10.2473/journalofmmij.127.111.
[42] Takeshita R, Yoshida I, Ueno K. Adsorption behaviour of phosphate ion on the iron (III) complexes of a chelating resin. Bull Chem Soc Jpn 1979;52 (9):2577–80. http://dx.doi.org/10.1246/bcsj.52.2577.
[43] Bockris JO, Tomlinson JW, White JL. The structure of the liquid silicates: partial molar volumes and expansivities. Trans Faraday Soc 1956;52:299. http://dx.doi.org/10.1039/tf9565200299.
[44] Sukenaga S, Haruki S, Nomoto Y, Saito N, Nakashima K. Density and surface tension of CaO–SiO_2–Al_2O_3–R_2O (R=Li, Na, K) melts. ISIJ Int 2011;51 (8):1285–9. http://dx.doi.org/10.2355/isijinternational.51.1285.
[45] Ohta Y, Morinaga K, Yanagase T. Application of hot-thermocouple to high temperature chemistry. Bull Japan Inst Met 1980;19(4):239–45. http://dx.doi.org/10.11311/jscta1974.13.90.
[46] http://www.factsage.com/.
[47] Waseda Y, Hirata K, Ohtani M. High-temperature thermal expansion of platinum, tantalum, molybdenum, and tungsten measured by X-ray diffraction. High Temp – High Press 1975;7(2):221–6.
[48] Shiraishi Y, Ikeda K, Tamura A, Saitô T. On the viscosity and density of the molten FeO–SiO_2 system. Mater Trans JIM 1978;19(5):264–74. http://dx.doi.org/10.2320/matertrans1960.19.264.
[49] Laboratories BE. General purpose silicone fluids; 2010. p. 1–6.
[50] Riebling EF. Structural similarities between a glass and its melt. J Am Ceram Soc 1968;51:143–9. http://dx.doi.org/10.1111/j.1151-2916.1968.tb11857.x.
[51] Courtial P, Dingwell DB. Densities of melts in the CaO–MgO–Al_2O_3–SiO_2 system. Am Mineral 1999;84:465–76. http://dx.doi.org/10.2138/am-1999-0401.
[52] Sumita S, Morinaga K, Yanagase T. Physical properties and structure of binary ferrite melts. Trans Jpn Inst Met 1983;24(1):35–41. http://dx.doi.org/10.2320/matertrans1960.24.35.